

LOCAL SEISMIC ACTIVITY MONITORED AT KING SEJONG STATION, ANTARCTICA

Duk Kee LEE, Yea Dong KIM, Sang Heon NAM and Young Keun JIN

Polar Research Center, Korea Ocean Research & Development Institute, Ansan P.O. Box 29, Kyung-Gi Province, Korea

Abstract: Source location estimation from single station earthquake data collected at King Sejong Station ($62^{\circ}13'31''\text{N}$, $58^{\circ}47'07''\text{W}$) from 1995 to 1996 provides seismic activity around King Sejong Station. Analysis of local events, less than 1.5° in angular epicentral distance, finds epicenters located near the Shackleton Fracture Zone, the South Shetland Platform, Deception Island, and North Bransfield Basin. Estimated magnitudes range from 2.2 to 4.5 on the Richter scale, averaging 4.0 in North Bransfield Basin, and 3.2 in the South Shetland Platform. Active seismicities along the NW-SE oriented gravity-low line, penetrating from the southwestern end of North Bransfield Basin into the South Shetland Trench, have been observed, averaging 3.3 on the Richter scale. No clear seismicity has been observed in the central segment of Bransfield Basin, although clear seismicities have been observed at both ends of Bransfield Strait including North Bransfield Basin and Deception Island. An active linear seismic zone along the South Shetland Platform, almost parallel to the South Shetland trench, is observed. The seismic activity along the South Shetland Platform is less than that in North Bransfield Basin.

key words: seismicity, focal mechanism, extension

1. Introduction

Major tectonic structures around the South Shetland Trench (SST) and Bransfield Strait (BS) include the Antarctic plate, Scotia plate, South American plate, and Nazca plate (Fig. 1). The boundaries between those major tectonic features form active seismic zones. The subducting Nazca plate under the Andes (South American plate) is responsible for the strong seismic activity in the western part of the South American plate (Fig. 1). The subducting South American plate under the Scotia plate near the South Sandwich Islands has supplied the extensional force in the back-arc near the South Sandwich Islands, showing strong seismic activity at the trench and back-arc. However, no clear seismicities have been observed in the SST and Central Bransfield Basin (CBB) according to the recent worldwide earthquake catalog (Fig. 2). Bransfield Strait (BS) lies between the South Shetland Islands and the Antarctic Peninsula. Two major transform systems are located near BS including the Shackleton Fracture Zone (SFZ) and the South Scotia Ridge (SSR) system (Fig. 2). The SFZ, located to the northeast of BS, shows transpressional motion (e.g., BARKER *et al.*, 1991). In contrast, the SSR, which shows transtensional motion, is located to the east of BS. The

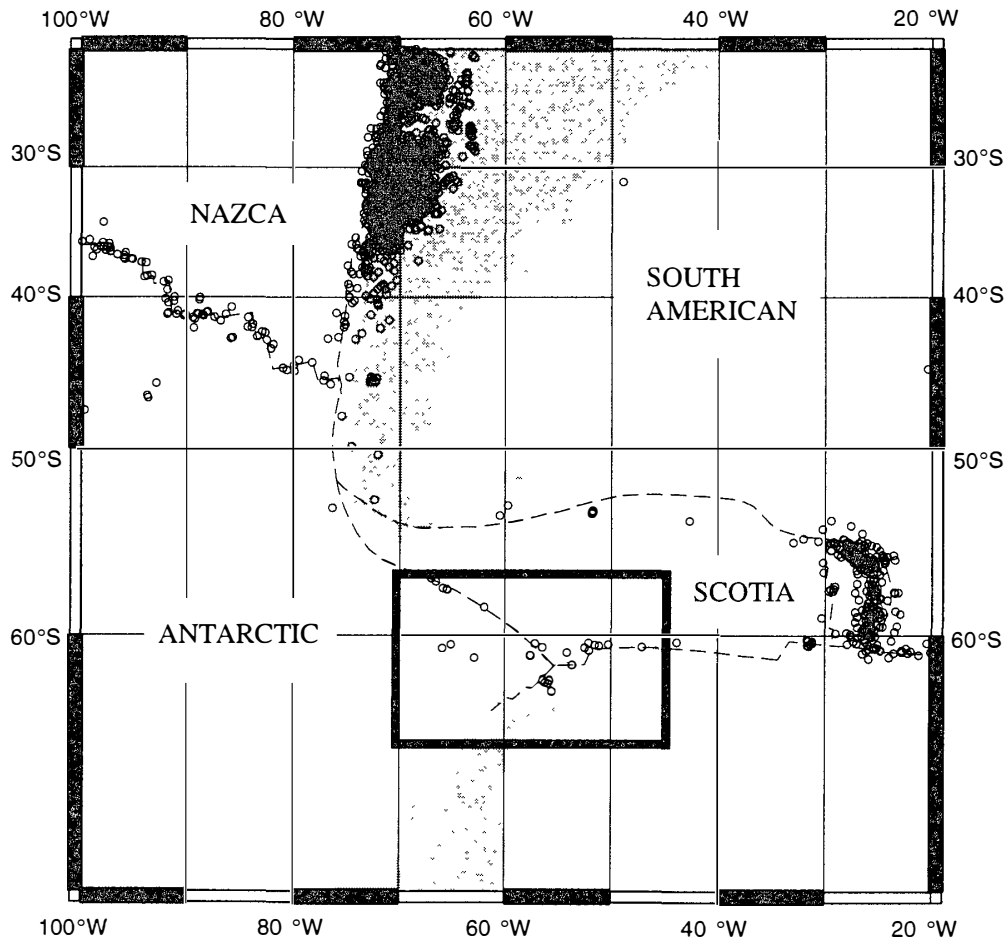


Fig. 1. A map showing seismic activity around King Sejong Station, Antarctica. Plate boundaries are drawn with dashed lines. Epicenters of earthquakes which occurred from 1991 to 1996 are plotted with empty circles. The Bransfield area is marked with a thick solid box.

intersection between the western end of the SSR and the southeastern part of the SFZ forms a large angle bend, showing highly irregular segment of the boundary near Elephant and Clarence Islands (KLEPEIS and LAWVER, 1996). The SST is located along the northern margin of the South Shetland Platform (SSP). The SSP is separated from the northern Antarctic Peninsula by BS. The SST is bordered by the SFZ and the Hero Fracture Zone (HFZ) on the northeast and southwest, respectively, as shown in Fig. 2. Successive ridge crest-trench collisions occurred along the Pacific margin of the Antarctic Peninsula from about 50 Ma to 4 Ma, causing termination phases of both spreading and subduction in the concerned plate segment (BARKER, 1982). The last surviving phases of the Antarctic-Phoenix spreading ridge lie to the northwest of the SST between the HFZ and the SFZ. The trench is the only remaining segment of the subduction zone that once extended to the entire Pacific Margin of the Antarctic Peninsula (HAWKES, 1981). Behind the South Shetland Islands that are believed to be a Jurassic-Quaternary magmatic arc, BS is located. BS has been believed to be formed by extension that separates the South Shetland Islands from the Antarctic Peninsula (BARKER, 1982; GAMBÔA and MALDONADO, 1990). The onset time of the Bransfield

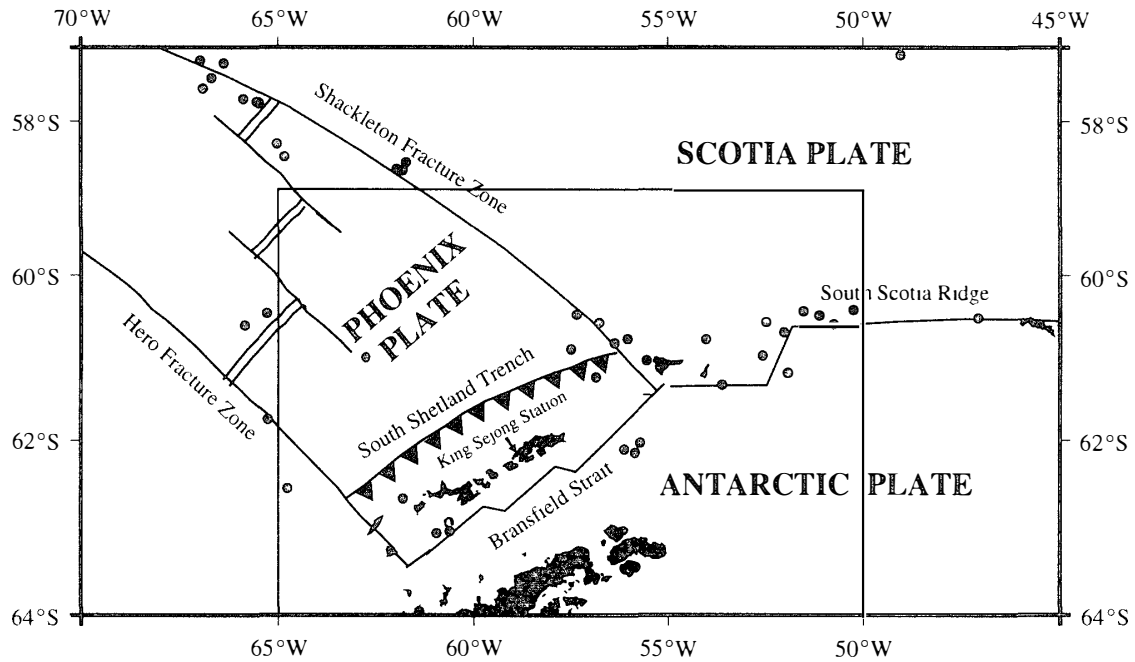


Fig. 2. A magnification of thick solid box shown in Fig. 1. Seismic activities reported from 1991 to 1996 are plotted with solid circles.

extension, however, is debated. Although different onset times ranging from 26 Ma to 1.3 Ma have been proposed (BARKER and DALZIEL, 1983; GONZÁLEZ-FERRÁN, 1985; PERRA *et al.*, 1988; BIRKENMAJER, 1992), the present extension regime seems to have begun 4 Ma ago, the terminating time of seafloor spreading at the Drake Rise (ROACH, 1978; BARKER and DALZIEL, 1983; BARKER *et al.*, 1991). LAWVER *et al.* (1996) strongly suggest present-day extension in Bransfield Strait considering the result of a multibeam survey in the Bransfield Strait. They also concluded that the cause of the present-day extension is still unclear.

One cause for the rifting in BS could be sinking of a subducting slab into the mantle beneath the SST (BARKER, 1982; BARKER *et al.*, 1991). Physiographic features of BS indicate that BS is a back-arc basin caused by active subduction along the SST (BARKER, 1982; JEFFERS and ANDERSON, 1990). Alternatively, many scientists have proposed that propagation of the stress field from the eastern Scotia Sea to Bransfield Basin (BB) is the cause of rifting in BB (*e.g.*, BARKER and AUSTIN, 1994). The axis of the topographic high in BS seems to merge into the major fault system of the transtensional Scotia-Antarctic plate boundary (KLEPEIS and LAWVER, 1996). Although large-scale seismological studies have been conducted in the area including the SST and CBB (PELAYO and WIENS, 1989; VILA *et al.*, 1992; KAMINUMA, 1995), seismic activities of these regions have never been resolved with high resolution. PELAYO and WIENS (1989) have studied relative plate motions by investigating the earthquake focal mechanism including BB. VILA *et al.* (1992) have observed active seismicity on Deception Island. KAMINUMA (1995) has included the seismic activity in BS. In the central segment of the BB system and the SST, however, the seismic activities have never been well documented. Detailed study of seismicity in the SST and CBB, therefore, might provide basic informa-

tion about the nature of the trench action as well as Bransfield extension and its relation to the neighboring tectonic settings.

In this paper, we analyze local events collected at King Sejong seismic station, Antarctica. The purpose is to determine the probable epicenters of events located near the SST and BB. Three different techniques have been applied to find the epicenters. First, rotations of two horizontal components of earthquake data from 0° to 360° have been done to find the backazimuths of the epicenters. Second, the covariance of two horizontal components (North and East) has been used to find the backazimuth. The third technique is to use cross-powers of P phase time windows between vertical and horizontal components. Only local earthquakes, less than 1.5° in epicentral distance, were used.

2. Data

King Sejong seismic station ($62^\circ 13' 31''$ S, $58^\circ 47' 07''$ W, 53 m) was installed in February 1989 by the Polar Research Center, Korea Ocean Research & Development Institute. This seismic station consists of an SS-1 Ranger seismometer, PS-2 analog drum recorder (Z component only), and 3-component SSR-1 digital recorder. The natural frequency of the SS-1 Ranger seismometer is about 1 Hz. Part of the data collected from 1995 to 1996 have been used to analyze the seismicity of BS. An example of data is shown in Fig. 3. Four events which occurred near King Sejong Station are plotted. The origin dates are written at the top of the figures. The bottom, middle, and top traces are vertical, north, and east components, respectively. Clear P -S

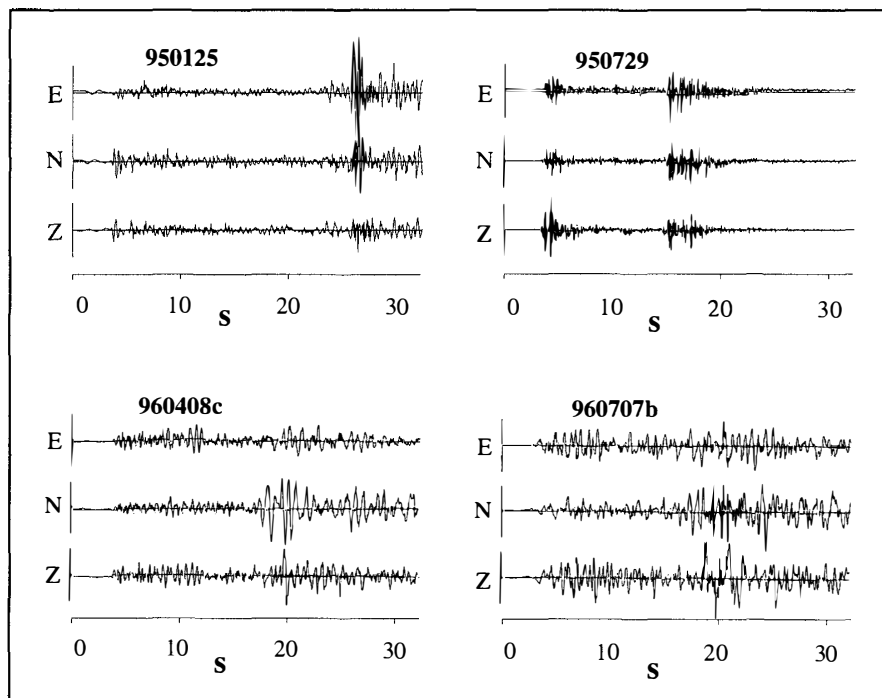


Fig. 3. Example of data. The origin dates are written at the top of the figures. Bottom, middle, and top traces are vertical, north, and east components respectively.

separation is seen.

3. Methods

3.1. Back-azimuth estimation

Many investigators have developed algorithms to find an epicenter for use with only single station three component data (MAGOTRA *et al.*, 1987; RUDD *et al.*, 1988; ROBERTS *et al.*, 1989; CHRISTOFFERSON *et al.*, 1988). King Sejong Station is the only digital seismic station available to study local seismicity (micro-seismicity) at the SST and in BS. Techniques to find epicenters with single station data, therefore, are critical to this study. The north and east components of an event can be projected onto the ray path direction from a receiver as follows, if the backazimuth angle is known. In matrix form, we have,

$$\begin{bmatrix} r \\ t \end{bmatrix} = U^T X = \begin{bmatrix} u_1 & u_2 \\ u_3 & u_4 \end{bmatrix} \begin{bmatrix} n \\ e \end{bmatrix},$$

where U^T is a normalized vector in the backazimuth direction. r and t are radial and tangential components, respectively. n and e are north and east components of the event. Along a radial component, a summation of amplitude power within a P phase time window is expected to be bigger than those in any other directions. That is,

$$\sum_t \sigma_r^2(t) \geq \sum_t \sigma_\theta^2(t),$$

where σ_r^2 and σ_θ^2 are amplitude powers within a P phase time window along a radial direction and arbitrary direction, respectively. σ_r^2 has the same meaning as $E[r^2]$, where $E[.]$ is the expectation. A backazimuth could be estimated by summing the amplitude power within a P phase time window using a grid search method. At each grid point ranging from 0° to 360° with 1° interval, two horizontal components can be projected into radial and tangential components assuming that each grid point is a backazimuth. Then, a summation of an amplitude power within P phase time window can be estimated to find a true backazimuth. There is an inherent 180° ambiguity in backazimuth estimation.

A seismic event detection and source location (SEDSL) algorithm (MAGOTRA *et al.*, 1987) has also been applied to find backazimuths. This algorithm is effective for detection of regional events ($< 20^\circ$), because a regional event has shallower incidence angle and so signals can be projected well onto two horizontal components. According to the SEDSL algorithm, the estimated covariance matrix ($C(t)$) can be defined by

$$C(t) = \begin{bmatrix} \hat{p}_n^2(t) & \hat{p}_{ne}(t) \\ \hat{p}_{ne}(t) & \hat{p}_e^2(t) \end{bmatrix},$$

where the elements of $C(t)$ can be estimated as follows

$$\begin{aligned} P_n^2(t) &= n^2(t), \\ P_e^2(t) &= e^2(t), \\ P_{ne}(t) &= n(t)e(t), \end{aligned}$$

where $n(t)$ and $e(t)$ are instantaneous north and east components, respectively. Maximum eigenvalues of $C(t)$ can be easily obtained by using the fact that the the following determinant must be zero.

$$\begin{vmatrix} P_n^2(t) - \lambda_M(t) & P_{ne}(t) \\ P_{ne}(t) & P_e^2(t) - \lambda_M(t) \end{vmatrix} = 0.$$

By solving the above quadratic equation, one can obtain maximum instantaneous eigenvalues ($\lambda_M(t)$) as follows.

$$\lambda_M(t) = \left[\frac{P_n^2(t) + P_e^2(t) + \sqrt{(P_n^2(t) - P_e^2(t))^2 + 4P_{ne}^2(t)}}{2} \right].$$

Backazimuth, therefore, can be evaluated from the maximum eigenvalue of the covariance matrix and corresponding eigenvectors. We have,

$$\begin{bmatrix} P_n^2(t) - \lambda_M(t) & P_{ne}(t) \\ P_{ne}(t) & P_e^2(t) - \lambda_M(t) \end{bmatrix} \begin{bmatrix} v_n(t) \\ v_e(t) \end{bmatrix} = 0,$$

where $v_n(t)$ and $v_e(t)$ are the north and east components of the eigenvectors, respectively. By taking $v_n(t)$ to be unity and solving the above equation, one can obtain relative eigenvectors as follows:

$$\begin{aligned} v_n(t) &= 1, \\ v_e(t) &= - \frac{[P_n^2(t) - \lambda_M(t)]}{P_{ne}(t)}. \end{aligned}$$

Since the meaning of the covariance of two horizontal components is the estimation of the seismic signal along the line in the northeast plane, the instantaneous backazimuth ($\phi(t)$) can be expressed as

$$\phi(t) = \tan^{-1} [v_e(t)].$$

Estimated backazimuth has an inherent 180° ambiguity. This ambiguity has been resolved by using cross-correlations among three orthogonal components. An example of this method is plotted in Fig. 4. Vertical, east, and north components of data are plotted in Fig. 4a. Clear P and S phases are seen. Instantaneous eigenvalues of the covariance are plotted at the bottom of Fig. 4b, while instantaneous backazimuths are plotted at the top of Fig. 4b. Note that the instantaneous backazimuths are nearly

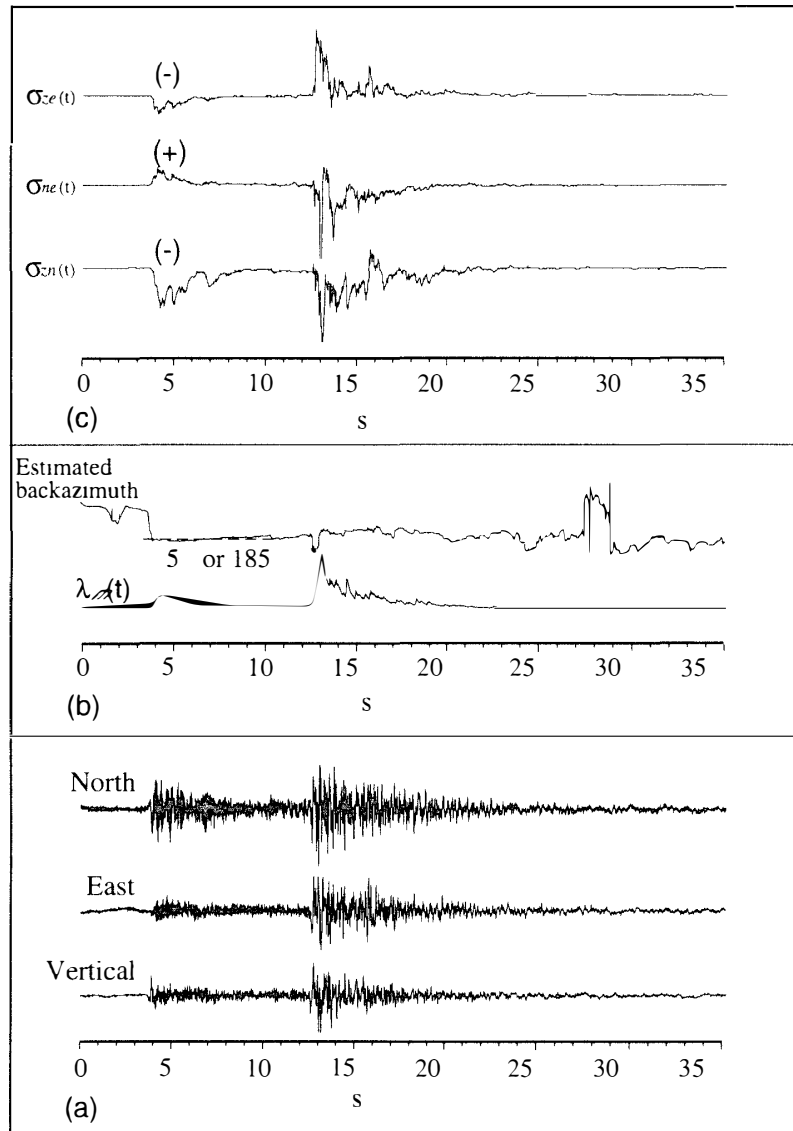


Fig. 4. An example of SEDSL algorithm (MAGOTRA *et al.*, 1987). The origin time of data is 01/28/95 0850:52.0. a) Vertical, east, and north components, b) eigenvalues of covariance of two horizontal components and estimated backazimuths, and c) cross-correlation among three components.

constant within the P phase time window. Also, clear onset of P and S phases is seen in the bottom trace of Fig. 4b. However, there is an inherent 180° ambiguity. This ambiguity can be resolved by using cross-correlations among the three components, under assumption that the positive polarities of the north, east, and vertical represent ground motion north, east, and up, respectively (Fig. 4c).

The third technique is to use part of the algorithm developed by ROBERTS *et al.* (1989). This technique finds the backazimuth by doing cross- and auto-correlations among three orthogonal components within a short time window of the P wave. Particle motion, $\chi(t)$, can be defined by:

$$\chi(t) = \begin{bmatrix} \chi_n(t) \\ \chi_e(t) \\ \chi_z(t) \end{bmatrix}.$$

Where χ_n , χ_e , and χ_z are the north, east, and vertical components for an event within a P phase time window. No P - S conversion phase is assumed to be included in the P phase time window. Then the three orthogonal components can be expressed in terms of the incoming P wave $P(t)$ and the noise $N(t)$ as follows for a given take-off angle θ and backazimuth ϕ .

$$\begin{aligned} \chi_n(t) &= P(t) \sin(\theta) \cos(\phi) + N_n(t), \\ \chi_e(t) &= P(t) \sin(\theta) \sin(\phi) + N_e(t), \\ \chi_z(t) &= P(t) \cos(\theta) + N_z(t), \end{aligned}$$

where $N_n(t)$, $N_e(t)$, and $N_z(t)$ are random noises on the three orthogonal components. The average cross powers over a given time window between the three channels become:

$$\begin{aligned} \langle \chi_z \chi_n \rangle &= \langle P^2 \sin(\theta) \cos(\theta) \cos(\phi) \rangle, \\ \langle \chi_z \chi_e \rangle &= \langle P^2 \sin(\theta) \cos(\theta) \sin(\phi) \rangle. \end{aligned}$$

Therefore, backazimuth (ϕ) can be expressed as:

$$\phi = \tan^{-1} \left(\frac{-\langle \chi_e \chi_z \rangle}{-\langle \chi_n \chi_z \rangle} \right).$$

The symbol $\langle \rangle$ represents averaging over the P phase time window. Also there is an 180° ambiguity in backazimuth estimation. Again, this ambiguity can be resolved by inspecting the cross-correlations among the three components. Another way of checking this ambiguity is to synthesize the vertical component from the two horizontal components within a P wave time window (ROBERTS *et al.*, 1989). The amplitude ratio of the vertical component to the radial component ($\cos\theta/\sin\theta$) can be expressed in terms of cross powers of amplitude because cross powers effectively remove the noise effect. The ratio (γ) becomes

$$\gamma = \sqrt{\frac{\langle \chi_z \chi_z \rangle}{\sqrt{(\langle \chi_n \chi_n \rangle^2 + \langle \chi_e \chi_e \rangle^2)}}}.$$

The vertical component (S_z) therefore can be synthesized using the estimated ratio as follows:

$$S_z(t) = -\gamma \{ \cos(\phi) \chi_n(t) + \sin(\phi) \chi_e(t) \} + N(t).$$

The ambiguity can thus be resolved by comparing the polarities of synthetics and data.

3.2. Distance, magnitude, and location estimation

P-S times have been measured for each event to estimate epicentral distances. Only local earthquakes have been analyzed to study possible seismic activities from the SST and BS. The identifications of the arrival phases within this epicentral range are ambiguous because the first arrivals could be any of P_n , P_mP , or P_g , depending on the source depth, epicentral distance, crustal thickness, and local velocity structure. Magnitude (Richter scale) was estimated using Wood-Anderson type amplitude. Finally epicenter locations have been measured using the estimated distance and backazimuth using the geocentric latitude and longitude relation.

4. Discussion

Seismic activity is well aligned with major tectonic features such as the SSR and the SFZ (Fig. 2) according to the worldwide earthquake catalog. Seismic activity has been concentrated near the intersection between the SSR, the SFZ, and BS, while little or no seismic activity has been observed along the SST and CBB. The rectangular box inside Fig. 2 has been magnified and focal spheres of the events from 1978 to 1994 (HARVARD CMT SOLUTION, 1997) are plotted in Fig. 5. Strike slip motions in the SFZ and the HFZ (event numbers 1, 9, 11, and, 12) near the SST may suggest that these events are not associated with subduction at the SST. Extensional seismicity associated with volcanoes is observed near Deception Island (DI) (event numbers 5 and 6). In the

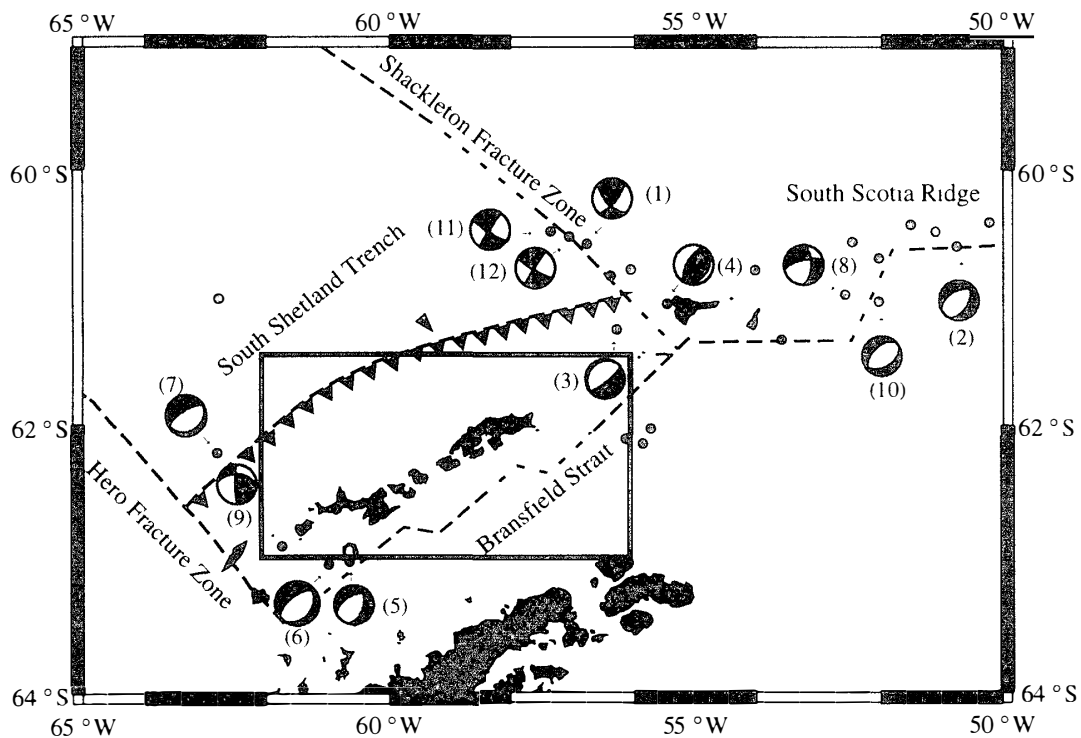


Fig. 5. Seismicities along the Shackleton Fracture Zone, South Scotia Ridge, and Bransfield Strait. Focal spheres are plotted as beach balls. The solid part of a focal sphere is an extensional scheme. The focal mechanism is from Harvard Centeroid Moment Tensor Solution (HARVARD CMT SOLUTION, 1997).

northeastern part of BS, seismicities at Elephant Island and North Bransfield Basin (NBB) are observed.

4.1. Seismicity in BB and DI

We could not find direct evidence of active seismicities in CBB based on the data collected at King Sejong Station. This does not necessarily mean that there is no extension in BS because we found 19 events which occurred at NBB and vicinity (marked as 'A' and 'DI' in Fig. 6). The free-air gravity contour lines shown in Fig. 6 are from KLEPEIS *et al.* (1996). NE-SW directed dashed lines in the upper right corner of Fig. 6 are faults (KLEPEIS *et al.*, 1996). Note that most of the events which occurred near the southwestern end of this fault system are within NBB (marked as 'A' in Fig. 6). The NW-SE directed lineament (plotted as dashed line in Fig. 6) is estimated from the regional gravity data (KLEPEIS *et al.*, 1996). The seismic activity seems to occur along this line, yet the cause of seismic activity along the NW-SE directed line is unclear. The events occurred in NBB (marked as 'A' in Fig. 6) is plotted in Fig. 7. Clear *P-S* separation is observed (top of Fig. 7). Depth phases (pP and sP) between *P* and *S* phases are observed. The result of forward modeling of travel times suggests that the focal depths of these events are less than 15 km. *P* wave time window marked by two vertical dashed lines is magnified and plotted at the bottom of Fig. 7. The waveforms of these events are similar. This suggests that these events were caused by similar fault plane actions within NBB. Also note that *S* waveforms are similar too. Although only one event from DI (Fig. 6) is observed in this research, several events from DI have been reported previously according to the worldwide earthquake catalog, showing the NE-SW directed extension axis (marked as '(5)' and '(6)' in Fig. 5).

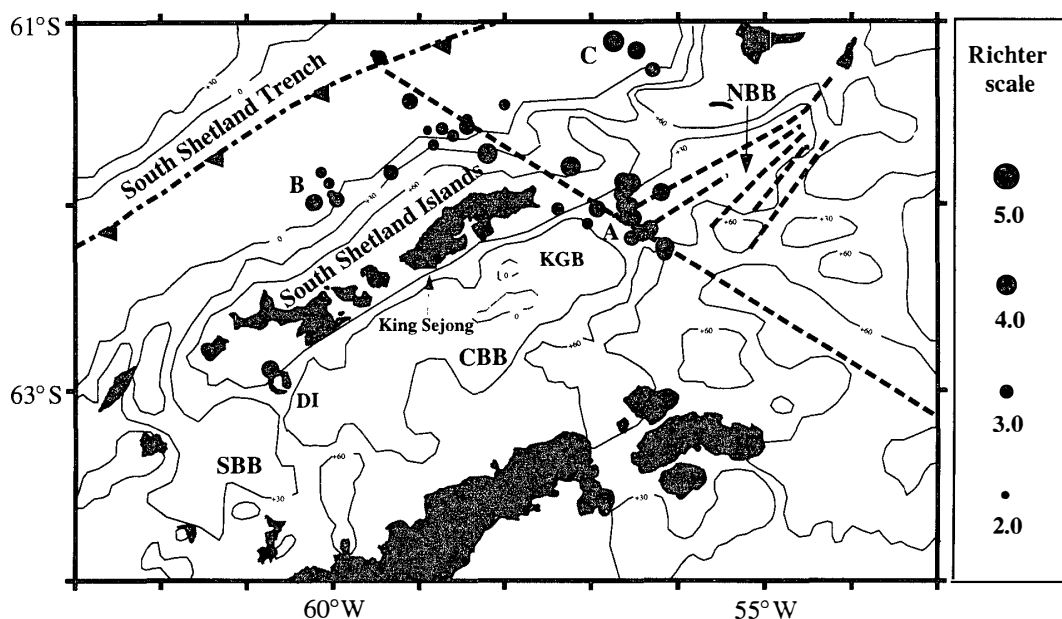


Fig. 6. Estimated epicenters from local events collected at King Sejong Station from January 1995 to September 1996. Solid circles represent epicenters.

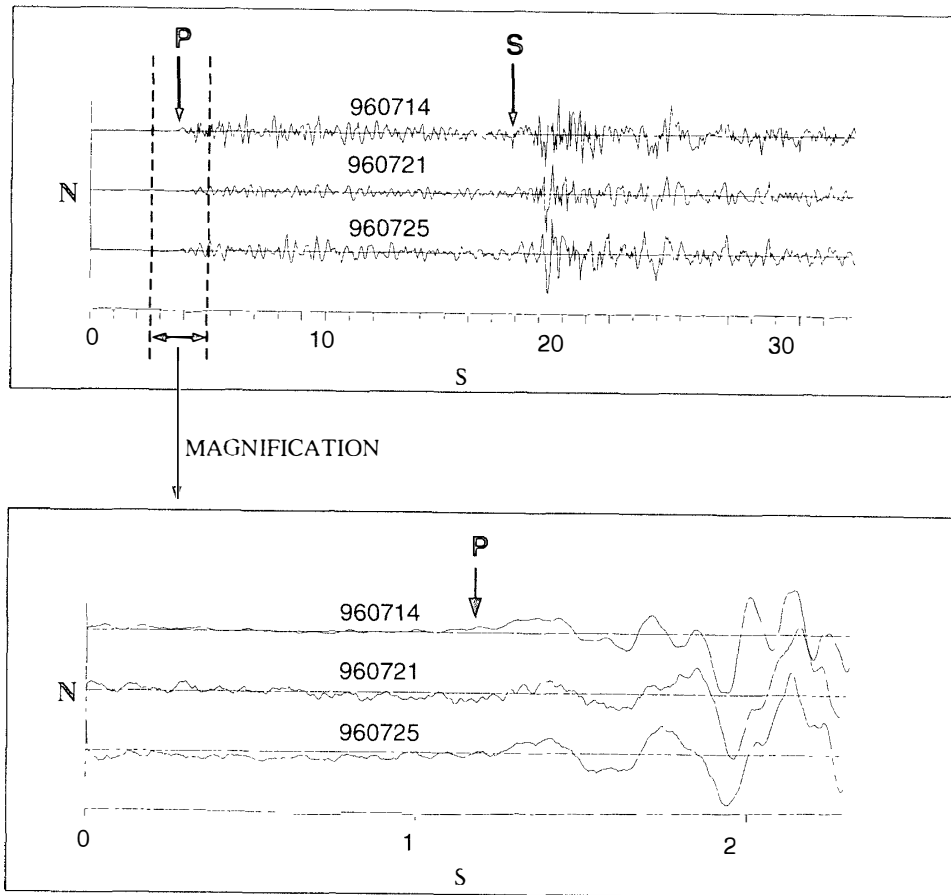


Fig. 7. An example of data from the area marked 'A' in Fig. 6. Clear onsets of P and S phases are observed. The P wave window is magnified and plotted at the bottom.

4.2. SST

Although no seismicity has been previously reported in detail along the South Shetland Platform (SSP), we found seismic activity along the SSP with an average magnitude 3.2 on the Richter scale (Fig. 6). The magnitudes of the earthquakes occurring along the SSP are generally small (average 3.2 in Richter scale) compared to those in NBB (average 4.0 on the Richter scale). This linear seismic zone along the SSP (between 'B' and 'C' in Fig. 6) is almost parallel to the SST, making us think that this seismicity might have originated from the result of the trench action along the SST. The fault plane solution, however, is unknown due to poor data. The cause of the seismicity along the SSP, therefore, is uncertain.

4.3. Errors

Errors in estimating epicenters for use with only single station data include the P-S time and backazimuth terms. P-S time estimation can be much influenced by the subjective identification of phases with different focal depths. Phase identification of local earthquakes used in this research is ambiguous because the first arrival could be any of Pn, P_mP or Pg, depending on the source depth, epicentral distance, crustal thickness, and local velocity structure. Theoretical travel times for different focal

Table 1. Comparison of epicenters between those estimated from this research and those in the world earthquake catalog.

Event name	Origin time	Source location		Backazimuth (degree)	Magnitude	Depth (km)
950726a	1995 07 26	58.628 S	61.965 W*	-24.0*	4.1*	10.0
	0144:17.3	59.150 S	61.420 W**	-25.0**	4.8**	
960210a	1996 02 10	60.918 S	57.493 W*	25.0*	4.7*	10.0
	1217:05.0	60.770 S	57.400 W**	24.0**	4.9**	
960707b	1996 07 07	62.023 S	56.336 W*	80.0*	4.3*	33.0
	0753:53.5	62.110 S	56.390 W**	84.0**	3.9**	
960707c	1996 07 07	62.503 S	55.550 W*	99.0*	4.2*	10.0
	1512:11.1	62.210 S	56.220 W**	91.0**	4.3**	
960709a	1996 07 09	62.482 S	55.528 W*	100.0*	4.3*	10.0
	0417:46.1	62.050 S	56.580 W**	82.0**	4.0**	
960719a	1996 07 19	61.998 S	56.342 W*	79.0*	4.1*	10.0
	1133:37.4	61.890 S	56.780 W**	73.0**	4.3**	

depths have been produced and compared to data to find the approximate P - S time. Although different local structure beneath the source area can also affect the P - S time measurement, this factor has been ignored because the epicentral distance is short and we assume that the source regions are rather homogeneous. Error range in estimating P - S time was within ± 1.0 s according to our data set. Also backazimuth estimation can significantly affect the result of epicenter estimation. Backazimuth estimation can be affected by the signal-to-noise ratio as well as the length of the P phase time window to be estimated. Different P phase time windows have been selected and processed using three different techniques to find the error range. In this estimation, no shear wave phases have been included. The error range in estimating the backazimuth is approximately $\pm 7^\circ$. Although the error in estimating epicenters for use with only single station data is significant, we still provide relatively accurate epicenters because the epicentral distances are generally short and the result from the data published in the worldwide earthquake catalog is in good accordance with our result. The epicenters determined by this research are compared with those from world earthquake catalog in Table 1. An asterisk, “*”, in Table 1 represents earthquake information from the worldwide earthquake catalog, while “**” denotes earthquake information derived from the present research. Magnitudes derived from this research are on the Richter scales, while those from the world earthquake catalog are in bodywave magnitudes.

5. Conclusions

Although BS is believed to be extending presently, no clear seismicity has been observed in CBB in this research. However, aseismicity in CBB could not be a direct evidence of termination of extension in BS because active seismicities in both ends of BS have been observed, including NBB and DI. The cause of the active seismic zone along

SSP is not clear because fault plane action is unknown, although the seismicities along the SSP have led us to believe that these seismic activities might originate from the result of trench action in the SST. Active seismic activities are observed along the NW-SE directed lineament that penetrates the western end of NBB. Further investigation of data (broad band data if possible) may illuminate in detail the nature of Bransfield extension as well as trench action and relation to the surrounding tectonic features.

Acknowledgments

The authors are grateful to the participants in the 8th and 9th Korea Antarctic Research Program, especially those who were in charge of the geophysical instruments at King Sejong Station. Special thanks are extended to Mr. Kyu-Jung KIM and Yong-Jeong YOON for their assistance.

References

- BARKER, P.F. (1982): The Cenozoic subduction history of the Pacific margin of the Antarctic Peninsula: Ridge crest-trench interactions. *J. Geol. Soc. London*, **139**, 787–801.
- BARKER, P.F. and DALZIEL, I.W.D. (1983): Progress in geodynamics in the Scotia Arc origin. *Geodynamics of the Eastern Pacific Region, Caribbean and Scotia Arcs*, ed. by R. CABRE. Washington, D.C., Am. Geophys. Union, 137–170.
- BARKER, P.F., DALZIEL, I.W.D. and STOREY, B.C. (1991): Tectonic development of the Scotia arc region. *The Geology of Antarctica*, ed. by R.J. TINGEY. Oxford, Clarendon Press, 215–248.
- BARKER, D.H.N. and AUSTIN, J.A., Jr. (1994): Crustal diapirism in Bransfield Strait, West Antarctica: Evidence for distributed extension in marginal-basin formation. *Geology*, **22**, 657–660.
- BIRKENMAJER, K. (1992): Evolution of the Bransfield basin and rift, West Antarctica. *Recent Progress in Antarctic Earth Sciences*, ed. by Y. YOSHIDA *et al.* Tokyo, Terra Sci. Publ., 405–410.
- CHRISTOFFERSON, A., HUSEBYE, E.S. and INGATE, S.F. (1988): Wavefield decomposition using ML-probabilities in modelling single-site 3-component records. *Geophys. J.*, **93**, 197–213.
- GAMBÔA, L.A.P. and MALDONADO, R. (1990): Geophysical investigations in the Bransfield Strait and in the Bellingshausen Sea, Antarctica. *Antarctica as an Exploration Frontier—Hydrocarbon Potential, Geology, and Hazards*, ed. by B. St JOHN. 127–141 (*Am. Assoc. Pet. Geol. Stud. Geol.*, No. 31).
- GONZÁLEZ-FERRÁN, O. (1985): Volcanic and tectonic evolution of the northern Antarctic Peninsula—Late Cenozoic to Recent. *Tectonophysics*, **114**, 389–409.
- HARVARD CMT SOLUTION (1997): IRIS Data Management Center, Washington.
- HAWKES, D.D. (1981): Tectonic segmentation of the northern Antarctic Peninsula. *Geology*, **9**, 220–224.
- JEFFERS, J.D. and ANDERSON, J.B. (1990): Sequence stratigraphy of the Bransfield Basin, Antarctica: Implication for tectonic history and hydrocarbon potential. *Antarctica as an Exploration Frontier—Hydrocarbon Potential, Geology, and Hazards*, ed. by B. St. JOHN. 13–29 (*Am. Assoc. Pet. Geol. Stud. Geol.*, No. 31).
- KAMINUMA, K. (1995): Seismicity around the Antarctic Peninsula. *Proc. NIPR Symp. Antarct. Geosci.* **8**, 35–42.
- KLEPEIS, K.A. and LAWVER, L.A. (1996): Tectonics of the Antarctic-Scotia plate boundary near Elephant and Clarence Islands, West Antarctica. *J. Geophys. Res.*, **101**, 20211–20231.
- LAWVER, L.A., SLOAN, B.J., BARKER, D.H.N., GHIDELLA, M., HERZEN, R.P.V., KELLER, R.A., KLINKHAMMER, G.P. and CHIN, C.S. (1996): Distributed, Active Extension in Bransfield Basin, Antarctic Peninsula: Evidence from Multibeam Bathymetry. *GSA Today*, **6** (11), 1–6.
- MAGOTRA, N., AHMED, N. and CHAEL, E. (1987): Seismic event detection and source location using single-station (three-component) data. *Bull. Seismol. Soc. Am.*, **77**, 958–971.
- PELAYO, A.M. and WIENS, D.A. (1989): Seismotectonics and relative plate motions in the Scotia Sea region.

- J. Geophys. Res., **94**, 7293–7320.
- PERRA, J.C., YANNEZ, G. and USAC WORKING GROUP (1988): Aeromagnetic survey of the Antarctic Peninsula and surrounding seas: Integration of the data obtained at different altitudes. Ser. Cient. Inst. Antart. Chil., **38**, 118–131.
- ROACH, P.J. (1978): The nature of back-arc extension in Bransfield Strait (abstract). R. Astron. Soc., Geophys. J., **53**, 165.
- ROBERTS, R.G., CHRISTOFFERSSON, A. and CASSIDY, F. (1989): Real-time event detection, phase identification and source location estimation using single station three-component seismic data. Geophys J., **97**, 471–480.
- RUDD, B.O., HUSEBYE, E.S., INGATE, S.F. and CHRISTOFFERSON, A. (1988): Event location at any distance using seismic data from a single, three-component station. Bull. Seismol. Soc. Am., **78**, 308–325.
- VILA, J., ORTIZ, R., CORREIG, A.M. and GARCIA, A. (1992): Seismic activity on Deception Island. Recent Progress in Antarctic Earth Science, ed. by Y. YOSHIDA *et al.* Tokyo, Terra Sci. Publ., 449–456.

(Received March 3, 1998; Revised manuscript accepted May 5, 1998)